Biosensors and Bioelectronics 74 (2015) 329–334

Contents lists available at ScienceDirect

Biosensors and Bioelectronics

journal homepage: www.elsevier.com/locate/bios

Gold nanoparticles-decorated graphene field-effect transistor biosensor for femtomolar MicroRNA detection

Bingjie Cai [a], Le Huang [b], Hong Zhang [c], Zhongyue Sun [a], Zhiyong Zhang [b,*], Guo-Jun Zhang [a,*]

[a] School of Laboratory Medicine, Hubei University of Chinese Medicine, 1 Huangjia Lake West Road, Wuhan 430065, PR China
[b] Key Laboratory for the Physics and Chemistry of Nanodevices, Department of Electronics, Peking University, No.5 Yiheyuan Road Haidian District, Beijing 100871, PR China
[c] Teaching and Research Office of Forensic Medicine, Hubei University of Chinese Medicine, 1 Huangjia Lake West Road, Wuhan 430065, PR China

ARTICLE INFO

Article history:
Received 3 April 2015
Received in revised form
26 June 2015
Accepted 27 June 2015
Available online 30 June 2015

Keywords:
MicroRNA detection
Graphene
Gold nanoparticles
Field-effect transistor biosensor
Peptide nucleic acid

ABSTRACT

Early detection is proven to be the best chance for successful cancer treatment. MiRNAs, as ideal biomarkers, can identify cancer in the early stage. Therefore, development of highly sensitive and selective detection methods for miRNA is still anticipated. Here we report on a gold nanoparticles (AuNPs)-decorated graphene field-effect transistor (FET) biosensor for highly sensitive, selective and label-free detection of miRNA. The AuNPs-decorated graphene FET biosensor was fabricated by drop-casting the reduced graphene oxide (R-GO) suspension onto the sensor surface, and subsequently decorating AuNPs onto the surface of R-GO. After peptide nucleic acid (PNA) probe was immobilized on the AuNPs surface, miRNA detection was carried out via PNA–miRNA hybridization. It was found that the developed FET biosensor was able to achieve a detection limit as low as 10 fM. In addition, the biosensor enabled an accurate distinction of complementary miRNA from one-base mismatched miRNA and non-complementary miRNA. What's more, this highly sensitive and selective assay was also applied to the detection of miRNA in serum samples, making it a potential method for diagnosis of gene-related diseases.

1. Introduction

MicroRNAs (miRNAs) are a family of short endogenous non-coding RNA molecules that have emerged as major regulators in the expression and function of eukaryotic genomes. Their regulation can have an effect on chromatin structure, chromosome segregation, transcription, RNA processing, RNA stability, and translation and so on (Carthew and Sontheimer, 2009; He and Hannon, 2004). Therefore, miRNAs play a key role in gene regulation, and miRNA dysregulation, resulting in a large number of diseases and disorders, such as pathogenesis of most human malignancies (Croce, 2009), virus-induced disorders (Nair and Zavolan, 2006), and neurodegenerative disease (Kim et al., 2007). MiRNAs have been evaluated as promising biomarkers because of their expression levels correlated with various diseases (Boeri et al., 2011; Iorio and Croce, 2009, 2012). It is thus of great importance to develop a sensitive, selective, simple and low cost miRNA detection method for biological research and clinical diagnosis.

Conventionally, miRNAs have been detected by northern blotting (Lagos-Quintana et al., 2001; Ramkissoon et al., 2006), molecular cloning (Takada et al., 2006), microarrays (Castoldi et al., 2008; Lee and Jung, 2011), real-time quantitative polymerase chain reaction (qRT-PCR) (Raymond et al., 2005; Li et al., 2009), etc. However, these methods suffer from some limitations, such as low throughput analysis, poor sensitivity, time and labor consuming. Therefore, it is highly desirable to develop an efficient, sensitive, rapid and low-cost platform for miRNAs detection.

Electrical detection is emerging as an attractive platform to detect biomolecules because of its compatibility, sensitivity and miniaturization (Zhang et al., 2009). There have been two main electrical detection methods, field-effect transistor (FET) and electrochemical biosensors, respectively, to detect nucleic acids. Gao and co-workers developed a highly sensitive and selective electrochemical biosensor for direct detection of miRNAs in serum by isothermal amplification cycle (Ren et al., 2013). Du et al. (2014) detected DNA by robust, reproducible and ratiometric electrochemical DNA sensors. Recently, the label-free FET biosensors have attracted much attention because they do not require

* Corresponding authors. Fax: +86 27 68890259.
E-mail addresses: zyzhang@pku.edu.cn (Z. Zhang), zhanggj@hbtcm.edu.cn (G.-J. Zhang).

http://dx.doi.org/10.1016/j.bios.2015.06.068
0956-5663/

electrochemical tags, but attain high sensitivity and selectivity (Cai et al., 2014; Dong et al., 2010; Star et al., 2006). Gao et al. (2013) reported a novel approach for DNA detection by applying rolling circle amplification based on silicon nanowire biosensor. Zhang et al. (2009) also utilized silicon nanowire biosensors for detecting miRNA. Star et al. (2006) used carbon nanotube network field-effect transistors for DNA detection. Graphene, a one-atom-thick two-dimensional (2D) sheet of sp^2-bonded carbon atoms, has drawn significant attention to scientific research owing to its unique and excellent properties, such as high carrier mobility, large active detection area, ease of functionalization and low intrinsic electrical noises and so on, making graphene more attractive than silicon nanowire or carbon nanotube. As a result, graphene-based FET biosensors have been developed in detecting nucleic acid (Cai et al., 2014; Dong et al., 2010; Xu et al., 2014; Zhang et al., 2013; Chen et al., 2013; Yin et al., 2012; Stine et al., 2010). For example, Xu et al. (2014) developed graphene FET biosensors for DNA detection with site-specific probe DNA immobilization. We have also reported the graphene FET biosensor for ultrasensitive DNA detection via PNA–DNA hybridization (Cai et al., 2014).

However, to date, all reported graphene FET biosensors have been used to detect DNA, but not miRNA. Here we propose a gold nanoparticles (AuNPs)-decorated graphene FET biosensor for highly sensitive and label-free detection of miRNA. In order to enhance the sensitivity of miRNA detection, we employ peptide nucleic acid (PNA) instead of DNA as a probe to capture the target miRNA because PNA has higher hybridization efficiency and lower background due to its neutral character and sequence-specific affinity and stability (Zhang et al., 2008; Hyrup et al., 1994). Besides employing the neutral PNA as the probe to enhance the detection sensitivity, decoration of nanoparticles is an additional method to enhance DNA detection sensitivity (Zhang et al., 2007; Chen et al., 2012). As known, since one nanoparticle can be modified with many PNA probes, the immobilized PNA probes are able to bind more target miRNA, thus increasing the hybridization efficiency. There are many kinds of nanoparticles to be chosen for the enhancement, while AuNPs are the commonly used one. AuNPs have been widely used for biosensors because of the well-known easy AuNP functionalization chemistry (Chen et al., 2012; Chang et al., 2013a, b). Ultimately, AuNPs are chosen to amplify the sensitivity in this work.

In this paper, a graphene FET biosensor chip is fabricated by micro manufacture processes. Reduced graphene oxide (R-GO) as the conducting material connects the adjacent electrodes. Then AuNPs are decorated on the R-GO surface and PNA probe is subsequently functionalized on the AuNP surface. Target miRNA is then introduced onto the biosensor surface to hybridize with PNA probe. The PNA–miRNA hybridization event is monitored by the electrical measurement. Moreover, the high selectivity of PNA–miRNA hybridization is demonstrated by using the complementary, one-base mismatched, and noncomplementary miRNA sequences, respectively. Finally, miRNA detection in serum samples is also realized by the fabricated FET biosensor.

2. Materials and methods

2.1. Materials

The HPLC-purified PNA probe and miRNAs were synthesized by Bio-Synthesis, Inc. (Lewisville, Texas) and Takara Biotechnology Co. Ltd. (Dalian, China), respectively. All PNAs and miRNAs were 22-mer in length. The sequence of the PNA probe is N-AACCACACAACCTACTACCTCA-C. The sequences of the miRNAs employed for hybridization are 5′-UGAGGUAGUAGGUUGUGUGGUU-3′ (let-7b, complementary), 5′-UGAGGUAGUAGGUUGUAUGGUU-3′ (let-7c, one-base mismatched), 5′-UAGCUUAUCAGACUGAUGUUGA-3′ (miR-21, noncomplementary), respectively. Graphite powder (99.99995%, 325 mesh) was purchased from Alfa Aesar Co., Ltd. (Tianjin, China). $HAuCl_4$, cysteamine hydrochloride, glutaraldehyde (GA), diethyl pyrocarbonate (DEPC), ethanolamine and RNaseZap were purchased from Sigma-Aldrich. All other reagents were ordered from Generay Biotech Co. Ltd. (Shanghai, China). Ultrapure water was obtained from a Millipore water purification system (Milli-Q Direct 8).

In order to minimize the effect of RNase on the stability of miRNAs, all the experiments involving miRNA were conducted in an RNase-free environment. All buffer solutions and water were treated with 0.1% DEPC and autoclaved. The chip surfaces were decontaminated with RNaseZap before introducing miRNAs.

2.2. Fabrication of graphene FET biosensors

The R-GO suspensions were produced using a foregoing method (Cai et al., 2014; Tung et al., 2009). The fabrication of the FET chip was completed by using the standard semiconductor technology. The diluted R-GO suspension was drop-casted onto the electrodes and thermally annealed at 150 °C for a few seconds in order to remove all hydrazine. After that, the R-GO biosensor chip was immersed in the Pirahna solution (7:3v/v conc. H_2SO_4/35% H_2O_2), and sonicated for 30 s to obtain few-layer R-GO, followed by thorough washing with DI water and drying with nitrogen.

2.3. AuNPs decoration on the R-GO films

$HAuCl_4$ solution was prepared at 10 mM concentration in DI water and an equal volume of ethanol, intended for better wetting of the R-GO surfaces. The graphene FET biosensor was immersed in $HAuCl_4$ solutions for 30 min followed by DI water rinsing and drying in a N_2 stream (Dong et al., 2010; Choi et al., 2002).

2.4. Immobilization of PNA on the AuNPs-decorated graphene surface

In order to immobilize PNA on the AuNPs surfaces, the AuNPs-decorated graphene FET was treated with a 10 mM cysteamine hydrochloride in DI water overnight at room temperature and washed with DI water, which could connect cysteamine with AuNPs through Au–S bonds and leave amino group on the terminal of the AuNPs surface. The cysteamine-modified FET was treated with 2.5% GA solution in water for 1 h, and thoroughly washed with water. 10 μM PNA was then introduced to the FET chip for 2 h at room temperature followed by being rinsed in sequence with 1 × PBS containing 0.2% SDS, 1 × PBS and DI water to remove the unreacted probe. By doing so, one aldehyde end of GA was covalently bound to the amino group of cysteamine, and the other aldehyde end of GA was bound to the amino group of PNA. Thus PNA was immobilized on the AuNPs surface. The device was then incubated with 100 mM ethanolamine solution (pH 9.0) for 1 h to prevent possible nonspecific binding events and then rinsed by DI water.

2.5. Hybridization

After the chip surface was treated with RNaseZap, PNA–miRNA hybridization was carried out by introducing appropriate concentration of complementary target miRNA solution onto the device and incubated for 30 min. Then the chip was rinsed in sequence with 1 × PBS containing 0.2% SDS, 1 × PBS, and DI water to remove the un-hybridized miRNA sequence and dried with N_2, in which the buffer solutions and DI water were treated with 0.1%

DEPC and autoclaved. The same procedure was repeated by using the one-base mismatched and noncomplementary miRNA sequences instead of the complementary target miRNA sequence to perform the hybridization with PNA probe.

2.6. Electrical measurements

The liquid-gated graphene FET devices were measured in a semiconductor parameter analyzer (Keithley 4200-SCS) coupled with a probe station (EverBeing BD-6). For I_{ds}–V_g (I_{ds} is the drain-source current, V_g is the gate voltage) curves measurements of the graphene devices, a silver wire was used as a gate electrode and a constant bias V_{ds}=0.1 V (the drain-source voltage) was applied.

2.7. Characterizations

A field emission-scanning electron microscope (FE-SEM) was used for SEM characterization of the device at a 15 kV acceleration voltage. AFM was conducted with a DI multimode scanning probe microscopy with IV controller.

3. Results and discussion

3.1. Detection principle

Fig. 1 illustrates the working principle of the AuNPs-decorated graphene FET biosensor for miRNA detection. As described in the previous report (Cai et al., 2014), the FET biosensor is fabricated on a SiO_2/Si substrate by the conventional macro-nano processing technologies, and the R-GO suspensions are prepared by a chemical reduction method (Cai et al., 2014; Tung et al., 2009). After the prepared R-GO is drop-casted onto the sensing channel as the conducting material, AuNPs are decorated on the R-GO surface through spontaneous AuNPs formation on graphene upon immersion of the graphene-modified FET biosensor chip in $HAuCl_4$ solution (Dong et al., 2010; Choi et al., 2002). Then, PNA probe is immobilized through the covalent binding between the amino group of PNA and an aldehyde group of GA, and the other aldehyde group of GA covalently binds to the amino group of cysteamine hydrochloride which connects AuNPs through Au–S bonding. After that, ethanolamine solution is used to prevent possible nonspecific binding events. Finally, the target miRNAs are introduced for hybridization with probe PNA, and then a silver wire is used as the reference electrode to realize a liquid-gated FET for electrical measurements. In principle, the complementary miRNA molecules cause n-doping to the devices due to the interaction between graphene and electro-rich nucleobases in miRNA (Cai et al., 2014; Dong et al., 2010; Xu et al., 2014; Chen et al., 2013; Lin et al., 2013; Manohar et al., 2008). The miRNAs detection can be measured through PNA–miRNA hybridization via monitoring the left-shift of I_{ds}–V_g curves of the devices.

3.2. Characterization

Fig. 2 shows the scanning electron microscopy (SEM) image of the graphene FET biosensor in the presence and absence of AuNPs. Bare R-GO sheet without AuNPs is illustrated in Fig. 2a. A few-layer R-GO sheet spanned across the drain and source electrodes, and the wrinkles of R-GO could be clearly seen. The bright dots on the R-GO surface were observed to be AuNPs in Fig. 2b, which were more visible in the inset image. From the inset, we could see many AuNPs decorated on the R-GO surface, indicating that AuNPs have been conjugated on the R-GO surface successfully. In addition, the optical images of the FET biosensor and the atomic force microscopy (AFM) image of the R-GO sheet were also provided in the supporting information (Figs. S1 and S2). As seen from Fig. S1, a single device containing six pairs of electrodes were presented and the sensing channels in the dashed rectangle were clearly seen. In Fig. S2, the R-GO sheet on SiO_2/Si substrate was seen to be smooth, while some wrinkles and folds which were brighter were also found. Two height profiles were made to demonstrate the thickness of the prepared R-GO sheet. Based on the height profiles, the thickness of the R-GO sheet was approximately 1.6 nm, suggesting the R-GO is few layers as expected.

3.3. Electrical properties

In order for a FET biosensor to detect a molecular event, the buffer solution must be used as the gate electrode. Fig. S3 shows I_{ds}–V_g curve of the bare R-GO on a SiO_2/Si substrate in the buffer solution (I_{ds}=0.1 V). As observed in Fig. S3, the difference between the drain and gate current suggested that the leakage current was negligible, meaning that the fabricated FET biosensor can work normally. To further investigate the electrical properties of the AuNPs-decorated graphene FET device, the typical I_{ds}–V_{ds} curves were obtained. As shown in Fig. S4, the drain-source current decreased with a slight reduction of the gate voltage, indicating that the response of the AuNPs-decorated graphene FET device is sensitive to the gate voltage (Chang et al., 2013b).

Next, to further demonstrate the successful decoration of AuNPs and immobilization of PNA on the device surface, the transfer curves of the graphene FET were obtained before and after the AuNPs decoration and PNA immobilization. In Fig. 3, the ambipolar characteristics of graphene could be clearly observed under ambient conditions. The p-type graphene was observed from

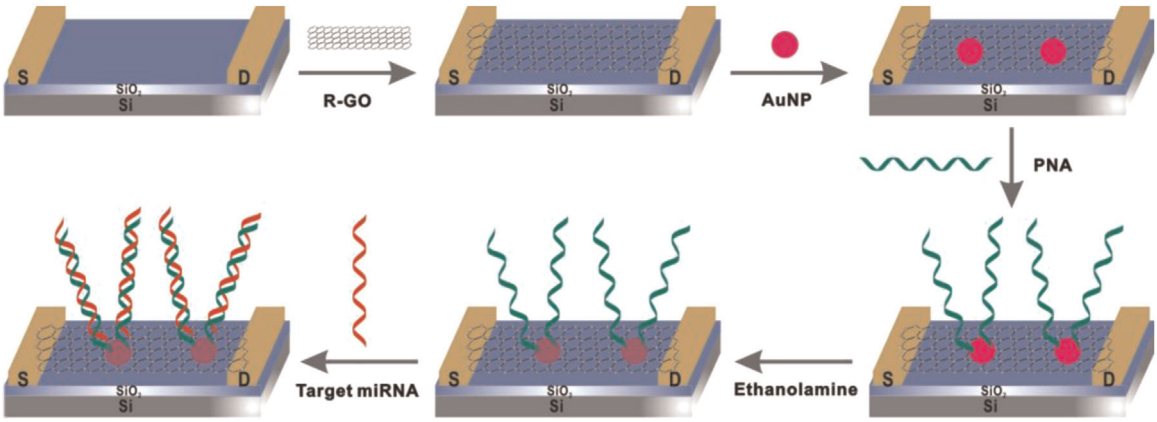

Fig. 1. Schematic illustration of the AuNPs-decorated graphene FET biosensor for miRNA detection.

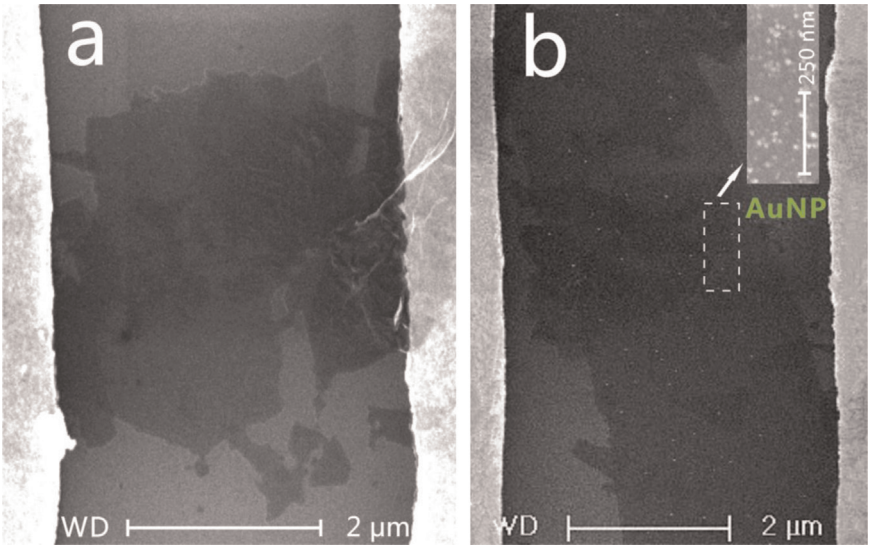

Fig. 2. SEM image of a single R-GO sheet in the absence (a) and presence (b) of AuNPs spanning across gold electrodes.

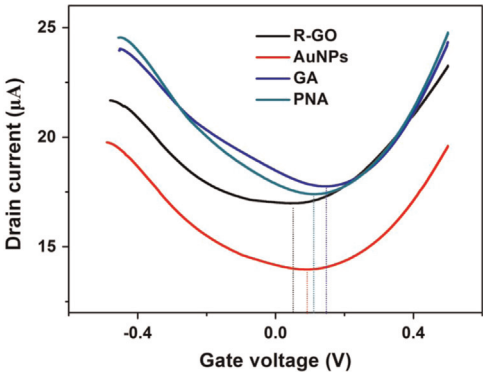

Fig. 3. The transfer curves of the graphene FET decorated with AuNPs, treated with GA and immobilized with PNA probe. (For interpretation of the references to color in this figure legend, the reader is referred to the web version of this article.)

the slight right shift of V_{CNP} (the gate voltage corresponding to the minimum conductance) in black curve due to adsorbates doping in the environment (Jung et al., 2008; Wang et al., 2009; Mao et al., 2010). The red curve obtained after AuNPs decoration shifted to right because of the p-doping of AuNPs, which is consistent with the result of other work (Dong et al., 2010; Choi et al., 2002; Kim et al., 2015). Again, the blue curve obtained after GA treatment shifted to right. However, compared to the blue curve, the green curve got after the immobilization of the PNA probe shifted to left. This is ascribed to the reason that PNA induces the same interaction between graphene and electro-rich nucleobases as miRNA does, resulting in the n-doping of the device. Thus the results suggest that the decoration of AuNPs and immobilization of PNA probe on the device surface are successful, as expected.

3.4. Selectivity

Previous work on DNA detection has shown that the PNA-functionalized graphene FET biosensor could be used for SNPs (single nucleotide polymorphisms) detection (Cai et al., 2014). The selectivity of the AuNPs-decorated graphene FET biosensor for miRNA detection was investigated by applying noncomplementary miRNA, one-base mismatched miRNA and complementary miRNA to the PNA-functionalized AuNPs-decorated graphene FET devices, respectively. The 1 × PBS, instead of the target miRNA, was conducted as the control test. Fig. 4a shows transfer curves of the PNA-immobilized AuNPs-decorated graphene FET biosensors incubated with 1 × PBS, 1 nM noncomplementary miRNA, 1 nM one-base mismatched miRNA and 1 nM complementary miRNA, respectively. As shown in Fig. 4a, the shift of V_{CNP} for complementary miRNA was much larger than that for 1 × PBS, noncomplementary miRNA and one-base mismatched miRNA, respectively. Fig. 4b summarizes the shift of V_{CNP} of the biosensors incubated with 1 × PBS and various miRNAs in Fig. 4a. The ΔV_{CNP} (namely the shift

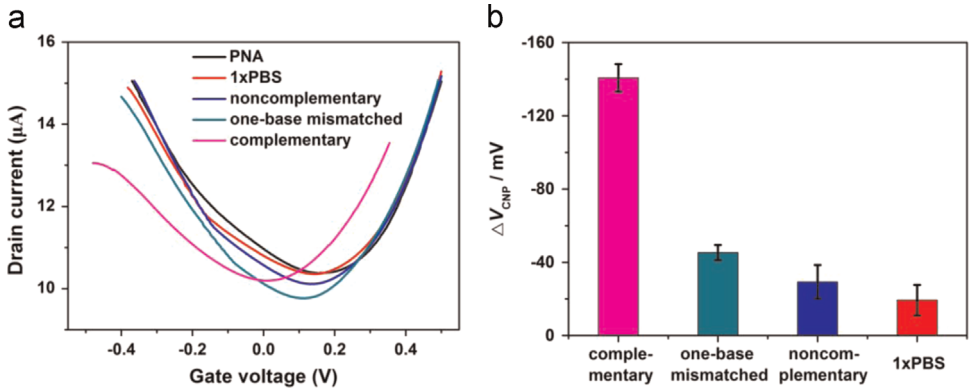

Fig. 4. (a) Transfer curves and (b) The shift of V_{CNP} of the PNA-immobilized AuNPs-decorated graphene FET biosensors incubated with 1 × PBS, 1 nM non-complementary miRNA, 1 nM one-base mismatched miRNA and 1 nM complementary miRNA, respectively. Error bars show the standard deviations of measurements taken from at least three independent samples.

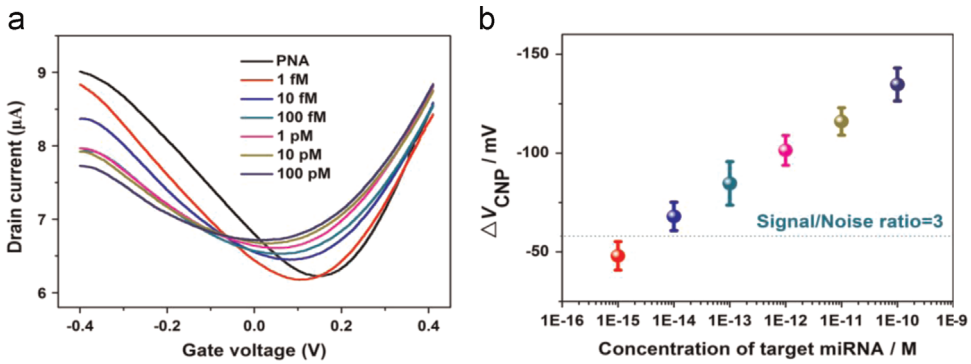

Fig. 5. (a) Transfer curves and (b) The shift of V_{CNP} of the PNA-immobilized AuNPs-decorated graphene FET biosensors hybridized with the complementary miRNA at a series of concentrations (1 fM, 10 fM, 100 fM, 1 pM, 10 pM and 100 pM). Dashed line represents the signal/noise ratio of 3 from the blank control test.

of V_{CNP} after incubated with 1 × PBS or miRNAs relative to V_{CNP} of PNA) of 1 × PBS, 1 nM noncomplementary miRNA, 1 nM one-base mismatched miRNA and 1 nM complementary miRNA was about −19.3, −29.3, −45.3 and −140.7 mV, respectively. The ΔV_{CNP} of 1 × PBS was defined as the noise level and the ΔV_{CNP} of non-complementary miRNA might be caused by a small amount of non-specific adsorption. The ΔV_{CNP} of one-base mismatched miRNA was much smaller than that of the target miRNA, mainly because of the unstable hybrid that would be unzipped and washed away (Tian et al., 2013). The data confirm that the hybridization is specific between PNA and target complementary miRNA and the biosensors can distinguish the complementary miRNA from one-base mismatched miRNA and non-complementary miRNA with good selectivity.

3.5. Sensitivity

In order to identify the sensitivity of the AuNPs-decorated graphene FET biosensor, various concentrations of complementary miRNAs were introduced to hybridize with PNA immobilized on the FET devices. From the Fig. 5a, we could see that the V_{CNP} of the devices shifted toward left with increased concentrations of the complementary miRNA from 1 fM to 100 pM. Fig. 5b shows the ΔV_{CNP} (namely the shift of V_{CNP} after hybridizing with different concentration of complementary miRNA relative to V_{CNP} of PNA) as a function of the concentrations of the complementary miRNA, which summarizes the left shift value of V_{CNP} at the corresponding concentrations of the complementary miRNA. Dashed line in Fig. 5b represents the signal/noise ratio of 3, which was obtained from the blank control test. Then, the detection limit of 10 fM rather than 1 fM was achieved based on the signal/noise ratio ≥ 3, which is 1 order magnitude lower than that of our previous work about PNA–DNA hybridization (Cai et al., 2014).

The sensitivity is affected by many factors, such as the quality of graphene, number of the immobilized probe, hybridization efficiency, concentration of buffer solution, materials of gate and so on. In the paper, both PNA as probe and AuNPs to amplify the signal were used. On one hand, PNA is a DNA mimic, which can enhance the detection sensitivity. Due to its neutral property, PNA has higher hybridization efficiency and lower background than DNA probe, because repulsion in PNA–DNA hybridization can be minimized. On the other hand, AuNPs can also amplify the detection signal. In this work, the method for depositing AuNPs on the RGO FET device involved dispersion of AuNPs in a mixture of ethanol and water. Such a methodology allowed formation of a very small AuNPs size, down to ca. 10 nm. If AuNPs are smaller, the surface areas are larger. Then more PNA probe can be immobilized on the AuNPs surface, thus enhancing the sensitivity.

To further verify that the high sensitivity was caused by AuNps decoration, different performance on the devices with and without gold decoration was compared. Fig. S5 shows the sensitivity of the graphene FET biosensor without gold decoration. It was found that the achieved limit of detection was 100 fM based on the signal/noise ratio ≥ 3, which is 1 order magnitude higher than that of the AuNPs-decorated graphene biosensor. The results demonstrate that the higher sensitivity can also owe to the enhancement of sensitivity by AuNPs.

3.6. Serum sample analysis

We made attempts to apply the AuNPs-decorated graphene FET biosensor for detecting target complementary miRNA in serum samples. The complementary miRNA was spiked to healthy human serum and diluted to different concentrations, as mentioned by the method of the reported work (Lu et al., 2014). Two different concentrations of miRNA in serum (1 fM and 10 fM) for miRNA detection were chosen, while serum without target miRNA was used as the control test. As illustrated in Fig. 6, the signal response of 10 fM miRNA in serum was higher than that of 1 fM miRNA in serum. Furthermore, it was observed that the signal response of serum with miRNA was larger than that of serum without miRNA. Thus, the AuNPs-decorated graphene FET biosensor show potential application in detecting miRNA in real samples.

4. Conclusions

In summary, we have developed the AuNPs-decorated graphene FET biosensor capable of achieving label-free, ultrasensitive and highly selective detection of miRNA. It was proven that AuNPs were successfully decorated on the graphene surface and the fabricated biosensor obtained a high sensitivity as well as a high selectivity based on PNA-miRNA hybridization. What's more, the

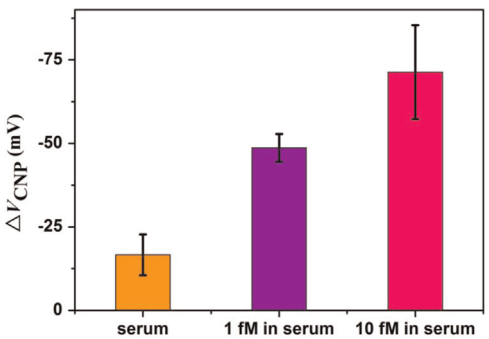

Fig. 6. The shift of V_{CNP} of the PNA-immobilized AuNPs-decorated graphene FET biosensors for detecting target complementary miRNA in serum samples.

developed biosensor was also able to detect target miRNA in serum sample. All of these advantages make the AuNPs-decorated graphene FET biosensor suitable for detecting targets in real samples, indicating its potential applications in disease diagnostics as a point-of-care tool.

Acknowledgments

This work was supported by the National Natural Science Foundation of China (Nos. 21275040 and 21475034), and the Natural Science Foundation of Hubei Province (No. 2013CFA061).

Appendix A. Supplementary material

Supplementary data associated with this article can be found in the online version at: http://dx.doi.org/10.1016/j.bios.2015.06.068.

References

Boeri, M., Verri, C., Conte, D., Roz, L., Modena, P., Facchinetti, F., Calabro, E., Croce, C. M., Pastorino, U., Sozzi, G., 2011. Proc. Natl. Acad. Sci. USA 108, 3713–3718.
Cai, B., Wang, S., Huang, L., Ning, Y., Zhang, Z., Zhang, G.J., 2014. ACS Nano 8, 2632–2638.
Carthew, R.W., Sontheimer, E.J., 2009. Cell 136, 642–655.
Castoldi, M., Schmidt, S., Benes, V., Hentze, M.W., Muckenthaler, M.U., 2008. Nat. Protoc. 3, 321–329.
Chang, J., Mao, S., Zhang, Y., Cui, S., Steeber, D.A., Chen, J., 2013a. Biosens. Bioelectron. 42, 186–192.
Chang, J., Mao, S., Zhang, Y., Cui, S., Zhou, G., Wu, X., Yang, C.H., Chen, J., 2013b. Nanoscale 5, 3620–3626.
Chen, K., Lu, G., Chang, J., Mao, S., Yu, K., Cui, S., Chen, J., 2012. Anal. Chem. 84, 4057–4062.
Chen, T.Y., Loan, P.T., Hsu, C.L., Lee, Y.H., Tse-Wei Wang, J., Wei, K.H., Lin, C.T., Li, L.J., 2013. Biosens. Bioelectron. 41, 103–109.
Choi, H.C., Shim, M., Bangsaruntip, S., Dai, H., 2002. J. Am. Chem. Soc. 124, 9058–9059.
Croce, C.M., 2009. Nat. Rev. Genet. 10, 704–714.
Dong, X., Shi, Y., Huang, W., Chen, P., Li, L.J., 2010. Adv. Mater. 22, 1649–1653.
Du, Y., Lim, B.J., Li, B., Jiang, Y.S., Sessler, J.L., Ellington, A.D., 2014. Anal. Chem. 86, 8010–8016.
Gao, A., Zou, N., Dai, P., Lu, N., Li, T., Wang, Y., Zhao, J., Mao, H., 2013. Nano Lett. 13, 4123–4130.
He, L., Hannon, G.J., 2004. Nat. Rev. Genet. 5, 522–531.
Hyrup, B., Egholm, M., Nielsen, P.E., Wittung, P., Norden, B., Buchardt, O., 1994. J. Am. Chem. Soc. 116, 7964–7970.
Iorio, M.V., Croce, C.M., 2009. J. Clin. Oncol. 27, 5848–5856.
Iorio, M.V., Croce, C.M., 2012. EMBO Mol. Med. 4, 143–159.
Jung, I., Dikin, D.A., Piner, R.D., Ruoff, R.S., 2008. Nano Lett. 8, 4283–4287.
Kim, J., Inoue, K., Ishii, J., Vanti, W.B., Voronov, S.V., Murchison, E., Hannon, G., Abeliovich, A., 2007. Science 317, 1220–1224.
Kim, K.W., Song, W., Jung, M.W., Kang, M.-A., Kwon, S.Y., Myung, S., Lim, J., Lee, S.S., An, K.-S., 2015. Carbon 82, 96–102.
Lagos-Quintana, M., Rauhut, R., Lendeckel, W., Tuschl, T., 2001. Science 294, 853–858.
Lee, J.M., Jung, Y., 2011. Angew. Chem. Int. Ed. Engl. 50, 12487–12490.
Li, J., Yao, B., Huang, H., Wang, Z., Sun, C., Fan, Y., Chang, Q., Li, S., Wang, X., Xi, J., 2009. Anal. Chem. 81, 5446–5451.
Lin, C.-T., Loan, P.T.K., Chen, T.-Y., Liu, K.-K., Chen, C.-H., Wei, K.-H., Li, L.-J., 2013. Adv. Funct. Mater. 23, 2301–2307.
Lu, N., Gao, A., Dai, P., Song, S., Fan, C., Wang, Y., Li, T., 2014. Small 10, 2022–2028.
Manohar, S., Mantz, A.R., Bancroft, K.E., Hui, C.Y., Jagota, A., Vezenov, D.V., 2008. Nano Lett. 8, 4365–4372.
Mao, S., Lu, G., Yu, K., Bo, Z., Chen, J., 2010. Adv. Mater. 22, 3521–3526.
Nair, V., Zavolan, M., 2006. Trends Microbiol. 14, 169–175.
Ramkissoon, S.H., Mainwaring, L.A., Sloand, E.M., Young, N.S., Kajigaya, S., 2006. Mol. Cell. Probes 20, 1–4.
Raymond, C.K., Roberts, B.S., Garrett-Engele, P., Lim, L.P., Johnson, J.M., 2005. RNA 11, 1737–1744.
Ren, Y., Deng, H., Shen, W., Gao, Z., 2013. Anal. Chem. 85, 4784–4789.
Star, A., Tu, E., Niemann, J., Gabriel, J.C., Joiner, C.S., Valcke, C., 2006. Proc. Natl. Acad. Sci. USA 103, 921–926.
Stine, R., Robinson, J.T., Sheehan, P.E., Tamanaha, C.R., 2010. Adv. Mater. 22, 5297–5300.
Takada, S., Berezikov, E., Yamashita, Y., Lagos-Quintana, M., Kloosterman, W.P., Enomoto, M., Hatanaka, H., Fujiwara, S., Watanabe, H., Soda, M., Choi, Y.L., Plasterk, R.H., Cuppen, E., Mano, H., 2006. Nucleic Acids Res. 34, e115.
Tian, K., He, Z., Wang, Y., Chen, S.J., Gu, L.Q., 2013. ACS Nano 7, 3962–3969.
Tung, V.C., Allen, M.J., Yang, Y., Kaner, R.B., 2009. Nat. Nanotechnol. 4, 25–29.
Wang, X., Li, X., Zhang, L., Yoon, Y., Weber, P.K., Wang, H., Guo, J., Dai, H., 2009. Science 324, 768–771.
Xu, G., Abbott, J., Qin, L., Yeung, K.Y., Song, Y., Yoon, H., Kong, J., Ham, D., 2014. Nat. Commun. 5, 4866.
Yin, Z., He, Q., Huang, X., Zhang, J., Wu, S., Chen, P., Lu, G., Chen, P., Zhang, Q., Yan, Q., Zhang, H., 2012. Nanoscale 4, 293–297.
Zhang, G.J., Chua, J.H., Chee, R.E., Agarwal, A., Wong, S.M., 2009. Biosens. Bioelectron. 24, 2504–2508.
Zhang, G.J., Chua, J.H., Chee, R.E., Agarwal, A., Wong, S.M., Buddharaju, K.D., Balasubramanian, N., 2008. Biosens. Bioelectron. 23, 1701–1707.
Zhang, J., Song, S., Wang, L., Pan, D., Fan, C., 2007. Nat. Protoc. 2, 2888–2895.
Zhang, X., Zhang, Y., Liao, Q., Song, Y., Ma, S., 2013. Small 9, 4045–4050.